R-04-54

Using the PCRaster-POLFLOW approach to GIS-based modelling of coupled groundwater-surface water hydrology in the Forsmark Area

Jerker Jarsjö, Yoshihiro Shibuo, Georgia Destouni
Dept. of Physical Geography and Quaternary Geology
Stockholm University

September 2004

Svensk Kärnbränslehantering AB
Swedish Nuclear Fuel
and Waste Management Co
Box 5864
SE-102 40 Stockholm Sweden
Tel 08-459 84 00
+46 8 459 84 00
Fax 08-661 57 19
+46 8 661 57 19

ISSN 1402-3091
SKB Rapport R-04-54

Using the PCRaster-POLFLOW approach to GIS-based modelling of coupled groundwater-surface water hydrology in the Forsmark Area

Jerker Jarsjö, Yoshihiro Shibuo, Georgia Destouni
Dept. of Physical Geography and Quaternary Geology
Stockholm University

September 2004

Abstract

The catchment-scale hydrologic modelling approach PCRaster-POLFLOW permits the integration of environmental process modelling functions with classical GIS functions such as database maintenance and screen display. It has previously successfully been applied at relatively large river basins and catchments, such as Rhine, Elbe and Norrström, for modelling stream water flow and nutrient transport. In this study, we review the PCRaster-POLFLOW modelling approach and apply it using a relatively fine spatial resolution to the smaller catchment of Forsmark. As input we use data from SKB's database, which includes detailed data from Forsmark (and Simpevarp), since these locations are being investigated as part of the process to find a suitable location for a deep repository for spent nuclear fuel.

We show, by comparison with independently measured, area-averaged runoff data, that the PCRaster-POLFLOW model produces results that, without using site-specific calibration, agree well with these independent measurements. In addition, we deliver results for four planned hydrological stations within the Forsmark catchment thus allowing for future direct comparisons with streamflow monitoring. We also show that, and how, the PCRaster-POLFLOW model in its present state can be used for predicting average seasonal streamflow.

The present modelling exercise provided insights into possible ways of extending and using the PCRaster-POLFLOW model for applications beyond its current main focus of surface water hydrology. In particular, regarding analysis of possible surface water-groundwater interactions, we identify the Analytic Element Method for groundwater modelling together with its GIS-based pre- and post processor ArcFlow as suitable and promising for use in combination with the PCRaster-POLFLOW modelling approach.

Furthermore, for transport modelling, such as that of radionuclides entering the coupled shallow groundwater-surface water hydrological system from possible deep repository leakage, a recent semi-analytical approach of Lindgren et al. *(Water Resources Research, vol. 40, 2004)* to modelling solute transport through the integrated groundwater-stream system of a catchment may, for instance, be a fruitful tool to use in combination with the PCRaster-POLFLOW surface-hydrological approach. For more detailed results on the actual evapotranspiration distribution (used as critical input for the PCRaster-POLFLOW modelling, for determination of the local precipitation surplus), the remote sensing model SEBAL (Surface Energy Balance for Land) appears to be powerful, because it is based on physical concepts, and does not rely on land use classification.

Contents

1 Introduction

PCRaster is a Geographical Information System (GIS) that has been developed at the faculty of Geographical Sciences of Utrecht University in the Netherlands. The system permits the integration of environmental process modelling functions with classical GIS functions such as database maintenance and screen display, and uses a single language for performing both GIS and process modelling operations (see /van Deursen, 1995/ and the summary of /Greffe, 2003/, for more details). Its main advantages include the high level of integration of GIS functionality for manipulation of input, results and model formulation, implying that new models (for instance, hydrological models, based on different model process assumptions and sub-system couplings) can be developed relatively fast and that the models also can be maintained with relative ease.

Recently, /Greffe, 2003/, /Darracq, 2003/, /Darracq et al, 2003/ and /Darracq and Destouni, 2004/ used PCRaster and the so-called POLFLOW catchment-scale hydrologic modelling approach /De Wit, 1999; 2001/ for modelling stream water flow and nutrient transport in the Norrström drainage basin. These studies showed that the model produced water flow and nutrient (nitrogen and phosphorous) transport results that were consistent with independent observations in monitoring stations at different locations within the drainage basin. Although several open hydrological research questions still remain, in particular regarding the coupling between surface water and groundwater, these results indicate that the PCRaster-POLFLOW model combination is capable of providing independent predictions of surface water hydrology in Swedish catchments.

Furthermore, the even more recent results of /Lindgren et al, 2004/, in terms of model tools for solute transport through the integrated groundwater-stream system of a catchment, provide a useful way forward for coupling with the PCRaster-POLFLOW model capabilities and addressing main hydrological research questions on groundwater-surface water interactions.

During 2002, SKB started site investigations at Forsmark and Simpevarp as part of the process to find a suitable location for a deep repository for spent nuclear fuel. In this context, /Rhén et al, 2003/ report a methodology for the development of hydrogeological site descriptive models within SKB's investigation programme. The report identifies the need to develop site-specific models of the surface water hydrology that are consistent with groundwater models of the same area. In the present work, we specifically investigate to which extent the capabilities of the PCRaster-POLFLOW tool box may fit the above needs, considering available data from the Forsmark site.

2 Objectives

2.1 Overall objective

Realistic and site-specific hydrological models require consistency between surface water and groundwater flows, implying a need for some degree of subsurface and surface water coupling in the process representations of the model. Overall objectives in the development of such coupled models are to obtain water mass balances that are consistent with observations of precipitation, evapotranspiration and water discharges, on local and catchment scales, and model representations of groundwater recharge and discharge zones that are realistic. Open research questions remain regarding, e.g. the necessary level of detail in the model representation of physical processes that underlie surface water-groundwater exchanges. However, it is clear that trustworthy models of surface water hydrology are necessary for the site-specific understanding of the potential biosphere effects of deep groundwater flows and the effects of surface hydrology on the deep flows, which motivates the specific objective of this project.

2.2 Specific objective and hypothesis

The specific objective of this study is to develop a GIS-based surface water model of the Forsmark area on the basis of available geographic, hydrological and hydrogeological data in SKB's database, using the PCRaster tool kit.

Our hypothesis is that we can use available, site-specific model parameters in the hydrologic process modelling approach of /van Deursen, 1995/ and /De Wit, 1999; 2001/ to provide a GIS-based surface hydrologic model of the Forsmark area that is consistent with independently reported hydrological data.

3 The numerical modelling approach

3.1 Overview

The PCRaster modelling approach requires a discretisation of the model domain into quadratic cells of equal size. The modelled area in Forsmark covers 10 km × 6 km, and the domain was discretised into 600,000 cells of size 10 m × 10 m. As input for the hydrological modelling module in PCRaster, each grid cell was assigned properties of elevation, precipitation, temperature, land cover, vegetation, aquifer porosity and aquifer capacity. Some of these basic properties, or input data, were pre-processed before running the hydrological modelling module. For instance, the ground slope was calculated on the basis of the elevation model. We used ESRI-Arc GIS 8.2 to handle the properties of the catchment in this pre-processing.

Figures 3-1 and 3-2 show the calculation scheme of the hydrological modelling module in PCRaster, used in this work in consistency with the POLFLOW model of /De Wit, 1999; 2001/. First, a precipitation surplus PS is calculated for each grid-cell (in mm/ year) as the difference between the precipitation, P, and actual evapotranspiration, E_a:

$$PS = P - E_a \quad (1)$$

which is illustrated in "Step 1" of Figure 3-1. Two different and independent methods are used in this study to estimate the E_a-term in Equation (1), in accordance with /Greffe, 2003/ and /Darracq, 2003/. The methods require different input data, as also indicated in the "Step 1"-textbox of Figure 3-1 (see Section 3.2 for further details on the calculation of P and E_a).

Following the quantification of PS according to Equation (1), it is assumed that a certain fraction of PS is available for groundwater recharge, according to a groundwater recharge index f_{gw}, which takes on values between 0 and 1, where 0 implies zero groundwater recharge and 1 implies groundwater recharge equal to PS. The remaining fraction $(1–f_{gw})$ is then available for surface water runoff from the grid-cell directly from the precipitation surplus in the cell, through fast surface runoff and soil interflow, to stream stretches within the cell. In addition, it is assumed that the groundwater recharge in each cell, in absence of any groundwater storage change within the considered time step / period (here primarily annual average conditions), gives rise to groundwater discharge, into the cell streams that equals the groundwater discharge in the cell.

Alternatively, for small grid cell sizes and cells far upstream in a catchment, significant groundwater discharge areas (streams) may not be assumed to exist within every cell and recharged groundwater in such cells may flow out from the cell as groundwater, rather than surface water runoff, and discharge into streams in cells located further downstream in the same sub-catchment (see Figure 3-2, discussed further in the following). A main model assumption is then that such possible groundwater runoff from small individual upstream cells follows the same main flow direction out from the cell as the stream water runoff (Figure 3-2), thus assuming the same sub-catchment areas and mean groundwater head slope directions as the surface water sub-catchments and directions of surface topographic slope, respectively.

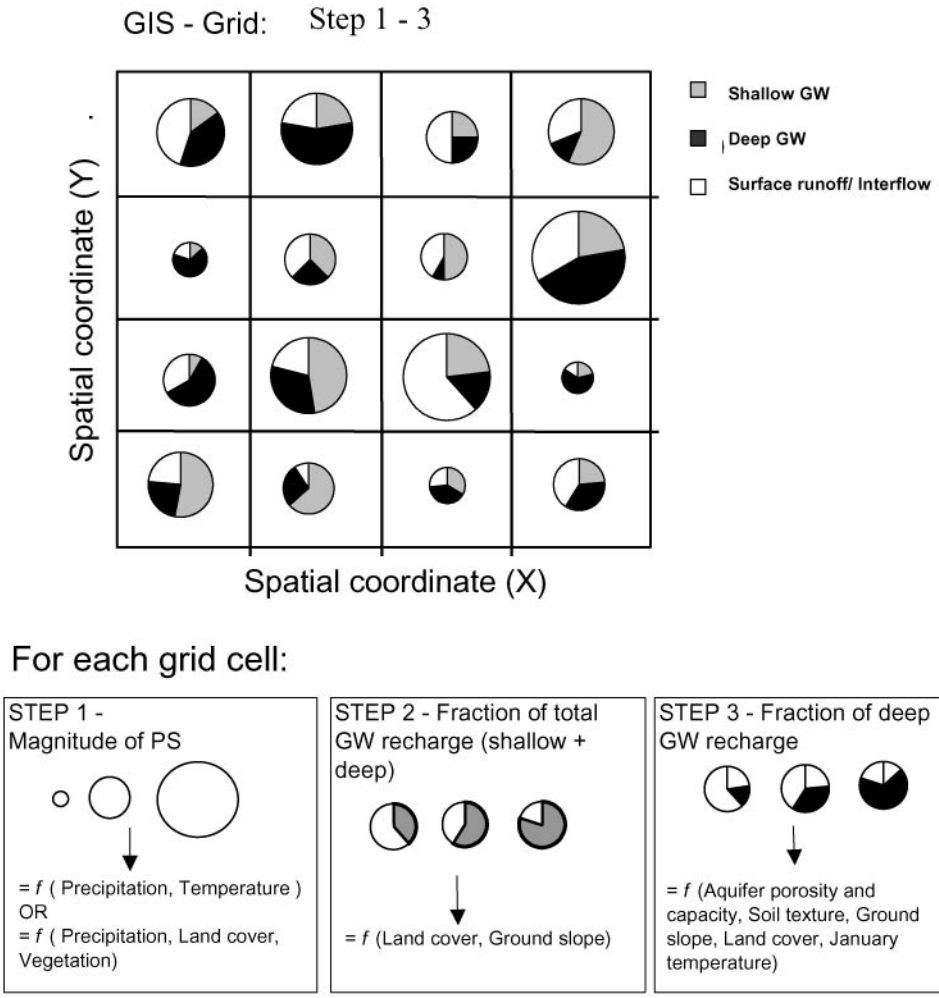

Figure 3-1. *Estimating the distribution of available precipitation surplus, PS (defined in Equation (1)) between recharge (in mm/year) of deep groundwater (black) and shallow groundwater ("tilted lines"), and surface water discharge (white) in each grid cell.*

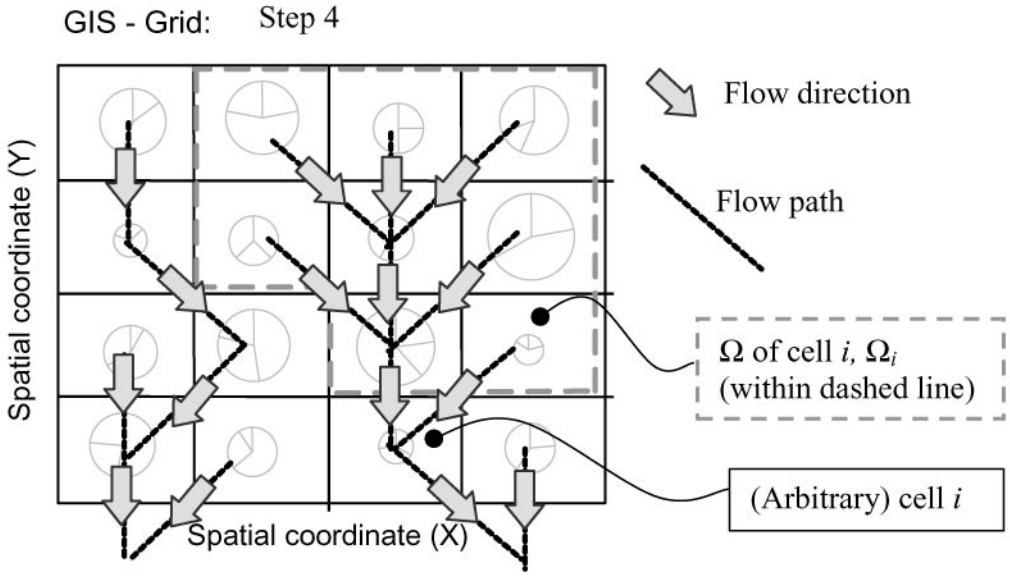

Figure 3-2. *Estimating the total water discharge, Q_i, through each grid cell i within upstream sub-catchment area Ω_i.*

The resulting total runoff of water precipitated within the cell, R, must be equal to PS at steady-state and is expressed (in mm/year) as the sum of the surface runoff and soil interflow contribution R_S, and the groundwater discharge contribution R_{gw}

$$R=R_S+R_{gw}=PS \quad (2)$$

Furthermore, the groundwater discharge R_{gw} must equal to the amount of precipitation surplus available for groundwater recharge, GW (illustrated by the grey areas in the "Step 2" box of Figure 3-1), which is calculated as

$$R_{gw}=GW=f_{gw}\cdot PS \quad (3)$$

and the surface runoff / soil interflow, R_S is calculated as the remaining amount of precipitation surplus available directly as stream water runoff (illustrated by the remaining white areas in the "Step 2" box of Figure 3-1)

$$R_S=(1-f_{gw})\cdot PS \quad (4)$$

The groundwater recharge index f_{gw} in Equations (3) and (4) is calculated by application of an empirical relation /from Wendland, 1992/ in each gridnode based on topographic slope and land cover data (see the separate Section 3.3). PCRaster is flexible and allows such empirical relations to be modified or changed if needed. It also allows for, e.g. division of the groundwater recharge, GW, into different categories such as shallow and deep groundwater recharge (illustrated by the "Step 3" box in Figure 3-1). The latter subdivision is achieved by adding equations that complement Equations (2) to (4). For example, /Meinardi et al, 1994/ used PCRaster and distinguished between shallow and deep groundwater recharge using the following additional relation:

$$GW=GW_S+GW_d=(f_{gw}-f_{dgw})\cdot PS+f_{dgw}\cdot PS \quad (5)$$

in which GW_d is the amount of precipitation surplus available for deep groundwater recharge (black areas in Figure 3-1), GW_S is the amount of precipitation surplus available for shallow groundwater recharge (dashed areas in Figure 3-1) and the fraction f_{dgw} of deep groundwater recharge is calculated according to Section 3.4.

In this study, we only distinguish the total groundwater recharge using Equation (3), and hence omit any further subdivision into shallow and deep groundwater recharge according to Equation (5). Both surface topography and land cover strongly influence the local groundwater recharge, however, we think that any further model improvements on the handling of groundwater require more attention to the coupling of, and exchange between, groundwater and surface water flows (see also the discussion section). The definition of, and division between, shallow and deep groundwater used by /Meinardi et al, 1994/ does not provide the means for performing such a coupling; we here present Equation (5) for the purpose of exemplifying that additional and different relation conceptualisations and equations can be incorporated into the PCRaster analysis toolkit.

Finally, for estimation of the total water discharge Q (L^3/T) through each grid cell, local flow directions of surface water and possibly also groundwater (arrows in Figure 3-2) are estimated on the basis of the digital elevation model. Each cell is then associated with a unique flow direction, into the neighbour with the lowest elevation. For instance, if the grid-lines are oriented in the N-S and E-W directions, the eight possible flow directions are: N, NE, E, SE, S, SW, W, and NW.

For each cell i, an associated sub-catchment area Ω_i is defined according to Figure 3-2, including all cells upstream of cell i, that contribute to Q_i through cell i, on the basis of all upstream defined flow directions. Using this definition of Ω_i (see also Figure 3-2), the average water discharge Q_i (L^3/T) through an arbitrary cell i during the considered simulation period (here primarily annual averages) is given by:

$$Q_i = \left(PS_i + \sum_i PS \right) \cdot A_{cell} \tag{6}$$

where A_{cell} is the cell area (all cells must have the same A_{cell} in PCRaster).

The flow Q represents the sum of surface water and groundwater discharge from each cell to downstream areas, with a main underlying assumption being that the sub-catchments and the mean flow directions for both the surface water and the groundwater discharge out from each sub-catchment are at least approximately the same; this assumption will generally be more valid for greater sub-catchments, i.e. the further downstream one goes within the main catchment, where main streams may be expected to represent discharge areas for groundwater, with the mean groundwater table sloping towards them, similarly to the topographic slope.

For determination of the magnitude of the surface water flow in relation to the groundwater flow contribution at any particular location within the Forsmark area, we used a hydrologic map indicating the locations of main streams. On the one hand, in cells where the headwater reaches of main streams first appear, such that these cells but not their upstream sub-catchments Ω_i include a main stream reach, the upstream groundwater flow contribution may be assumed to discharge into, and directly add to, the total stream water flow of the stream reach in cell *i*. The groundwater discharge is then added either totally where the headwater reaches first appear (for simplicity), or partly with some part then continuing to flow as groundwater flow into further downstream cells, contributing to stream water flow there. For instance, the groundwater discharge can be distributed along the stream according to some distribution function, or based on more detailed off-line groundwater simulations.

In either case, if a main stream is present in the considered cell, its stream water flow will generally be much greater than the groundwater flow not discharging into the stream, and hence the flow value Q_i given by Equation (6) can then on sound physical grounds be assumed to provide a good estimate of the stream water flow. In addition, in the present Forsmark application, we are primarily focused on water discharges in relatively large sub-catchments and coastal outlets of the Forsmark catchment, for which Q_i can be assumed to consist almost only of stream water. On the other hand, if a main stream and thereby a clear groundwater discharge area is not present in the considered cell and its sub-catchment area Ω_i, then the groundwater flow, $Q_{i,GW}$, can be at least approximately quantified by substituting PS for $GW=f_{gw}\cdot PS$ in Equation (6). The corresponding surface water flow $Q_{i,,S}$ occurring in minor streams or as overland flow within the cell and its sub-catchment Ω_i, is then obtained by substituting PS for $R_S=(1-f_{gw})\cdot PS$ in Equation (6).

3.2 Precipitation surplus PS(E_a,P)

The long-term, average, precipitation surplus PS equals the difference between the precipitation, P, and actual evapotranspiration, E_a (see Equation (1)). In PCRaster, PS is calculated for each gridnode within the model area, which hence requires a *precipitation map* and *a map of the actual evapotranspiration*. For calculating the evapotranspiration map, two different and independent methods were used. However, both methods imply that considerable simplifications need to be made, and we therefore specifically evaluate the differences in results between them (see further the results section).

In method (**i**), E_a is assumed to be a relatively simple function of P and the potential evapotranspiration E_p (from /Turc, 1954/ and used, e.g. by /Meinardi, 1994/ and /De Wit et al, 2000/):

$$E_a = \frac{P}{\sqrt{0.9 + \frac{P^2}{E_p^2}}} \tag{7}$$

in which E_p is directly related to the annual mean temperature T according to /Langbein, 1949/:

$$E_p = 325 + 2 \cdot T + 0.9 \cdot T^2 \tag{8}$$

where P and E_p are expressed in mm/year and T is expressed in °C and the parametric constants in (7)–(8) have appropriate associated units and account only implicitly for the effects of soil and vegetation on potential and actual evapotranspiration.

By contrast, in method (**ii**) E_a is related empirically but explicitly to different soil and vegetation conditions. Table 3-1 shows empirically calibrated E_a-values for different soil and vegetation conditions in German catchments /Wendland, 1992/. In the Forsmark catchment application of this study, we make use of the calibrated E_a-values listed in Table 3-1, thus neglecting at this stage potential differences in ambient conditions between Sweden and Germany. In cases when the estimated E_a was greater than 90% of the local P-value (using either method (i) or (ii)), the relation $E_a = 0.9 \cdot P$ was used instead of the method (i) or (ii) estimation.

Table 3-1. E_a-values as a function of soil texture and land cover (method (ii); /Wendland, 1992/).

Soil texture: Land cover:	E_a(mm/year) Forest	Water/ wetland	Other land cover
Very fine	570	600	550
Fine	550	600	470
Medium fine	530	600	423
Medium	475	600	375
Coarse	450	600	325
Water	600	600	600

3.3 Total groundwater recharge

The total groundwater recharge index f_{gw} is estimated on the basis of the land cover map and the topographic ground surface slope (sl) according to the empirical expression of /Wendland, 1992/:

$$f_{gw} = \begin{cases} 0.0001 & (\text{if landcover type} = 5; \text{water}) \\ 0.5 & (\text{if landcover type} = 4; \text{wetland}) \\ 1/\left(1 + 3 \cdot (sl + 0.0001)^{0.6}\right) & (\text{else}) \end{cases} \quad (9)$$

where the slope sl is derived from the elevation map.

3.4 Deep groundwater recharge

/Meinardi et al, 1994/ suggested the following empirical relation for estimation of the deep groundwater recharge index f_{dgw}:

$$f_{dgw} = f_{dgw}^{aq} \cdot f_{dgw}^{so} \cdot f_{dgw}^{lc} \cdot f_{dgw}^{tj} \cdot \left(1 - (sl + 10^{-7})^{0.4}\right) \quad (10)$$

where f_{dgw}^{so} depends on the soil texture, f_{dgw}^{lc} depends on the land cover, and f_{dgw}^{tj} depends on the average degree of soil freezing, as parameterised by use of the average January temperature, with empirically calibrated parameter values listed in Table 3-2a–c. Furthermore, f_{dgw}^{aq} depends on the aquifer capacity and is given in Table 3-3. As in Equation (9), the slope sl is derived from the elevation map. We have included Equation (10) in this report for the purpose of exemplifying how different equations and relations can be incorporated into the PCRaster analysis toolkit. However, as stated and motivated in Section 3.1, the equation has not been used for the present particular study of the Forsmark catchment.

Table 3-2. Values of (a) f_{dgw}^{so} as a function of soil texture, (b) f_{dgw}^{lc} as a function of land cover, and (c) f_{dgw}^{tj} as a function of January temperature /Meinardi et al, 1994/.

(a) Soil texture (so)	f_{dgw}^{so}	(b) Land cover (lc)	f_{dgw}^{lc}	(c) January temperature (tj)	f_{dgw}^{tj}
Very fine	0.05	1. Built-up	0.4	>0	1.0
Fine	0.25	2. Open land	0.92	0 to –4	0.90
Medium fine	0.5	3. Forest	1.0	–4 to –8	0.75
Medium	0.75	4. Wetland	0.10	–8 to –12	0.50
Coarse	0.95	5. Water	10–6	–12 to –16	0.25
Water	0.1			<–16	0.10

Table 3-3. Values of f_{dgw}^{aq} as a function of aquifer properties.

Aquifer class (SGU)	Aquifer type	Capacity (l/h)	f_{dgw}^{aq}
1003	Igneous rock	6,000–20,000	0.45
1004	Igneous rock	2,000–6,000	0.40
1005	Igneous rock	600–2,000	0.30
1006	Igneous rock	<600	0.10

3.5 Groundwater residence times

PCRaster can also handle and quantify shallow and deep groundwater residence times (RT_{sgw} and RT_{dgw}, respectively), see e.g. summary of /Greffe, 2003/. However, we will not in the present study analyse residence times, since the focus is on water flow rather than on solute transport.

4 Application Forsmark: The catchment and input data

The location of the studied Forsmark catchment is shown in Figure 4-1, along with the location of nearby SMHI monitoring stations used for obtaining temperature data and precipitation data. The main input data used for the PCRaster modelling are summarised below, along with short lists indicating the relation between input variables and model variables.

Figure 4-1. *Location of the studied Forsmark catchment and nearby SMHI meteorological stations.*

4.1 Digital elevation model and streams

The elevation-values of the original digital elevation model were lowered (by 3 m) at the location of streams, in order to ensure that the developed model reproduces the stream pattern correctly. The stream outlet locations were identified by comparing the catchment boundary, coastlines, and elevation data. Cells at the outlets were then lowered so that they would collect all the precipitation input that fall within the catchment area. In the next step, pits (or sinks) within the catchment were identified and filled by use of the "Hydrology Modelling" extension tool in ArcMap. Finally cells located next to the catchment boundaries were elevated to prevent any water exchanges across the boundaries. This processed digital elevation model was used to obtain data on the slope of the ground-surface and local flow directions. In summary, the ground-surface slope influences:

- Calculated flow directions.
- Calculated catchment and sub-catchment boundaries.
- Fraction of deep groundwater recharge (f_{dgw}), see Equation (10).
- Total fraction of groundwater recharge (f_{gw}), see Equation (9).
- Shallow groundwater residence times.

For orientation, the delineated catchment boundaries and locations of streams and stream outlets are shown in Figure 4-2. The figure also indicates the locations of the (planned) SKB hydrological measurement stations VP1, VP2, VP3 and VP4.

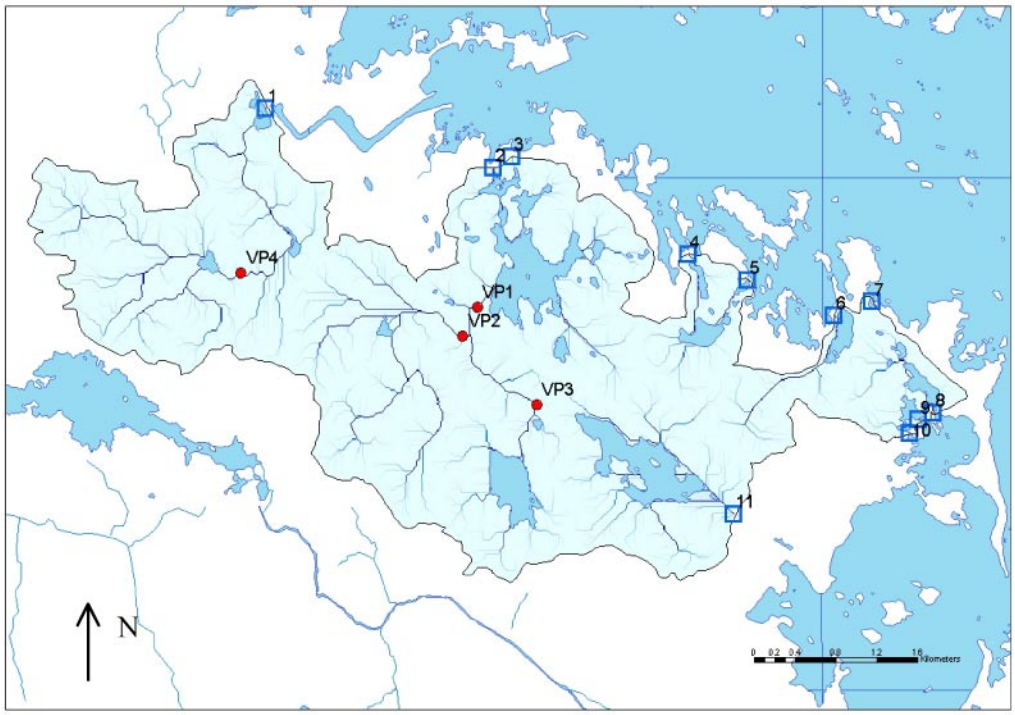

Figure 4-2. *Location of catchment boundary (black line), streams (blue lines), stream outlets (1 to 11) and planned hydrological measurement stations (VP1 toVP4).*

4.2 Precipitation

Annual average precipitation was calculated on the basis of four SMHI meteorological stations (Lövsta, Risinge, Untra, and Örskär; Figure 4-1) for the period 1961–1990. Using the spline function in ArcGIS Spatial Analyst, these four data points were interpolated to derive annual average precipitation input for the PCRaster calculation, as shown in Figure 4-3a, in which the rectangle represents the modelling area. For the case of average seasonal water discharge calculations, precipitation data was initially averaged over each month during the 1961–1990 period, and then the monthly averaged precipitation was summed up to derive average summer period precipitation (June to September) and average winter period precipitation (October to May) at the four stations.

The following model parameters are influenced by the precipitation P:

- $PS(E_a,P)$.
- E_a calculated according to method (**i**), see Equations (7) and (8).

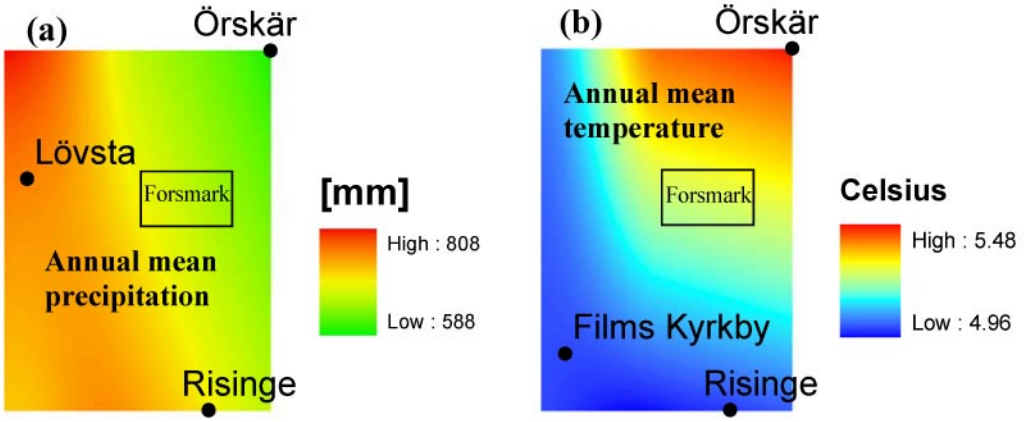

Figure 4-3. *Interpolated annual average (a) precipitation, and (b) temperature for the Forsmark model area, and the location of the closest SMHI measurement stations.*

4.3 Temperature

In the same manner as described in the precipitation section above, the average temperatures were calculated on the basis of the four nearest SMHI stations Films kyrkby, Risinge, Untra and Örskär (see Figure 4-1). Figure 4-3b shows the resulting interpolated annual average temperature for the Forsmark model area (indicated with a rectangle in Figure 4-3b).

The following model parameters are influenced by the temperature:

- E_a calculated according to method (**i**), see Equations (7) and (8).
- Fraction of deep groundwater recharge (f_{dgw}), see Table 3-2 and Equation (10); not used for the results presented in this report.

4.4 Evapotranspiration

Two independent methods for calculation of average annual evapotranspiration E_a were used in this work, namely

- **Method (i)** – as a function of potential evapotranspiration E_P (T), according to Equations (7) and (8).
- **Method (ii)** – as a function of soil texture and land cover, according to Table 3-1.

The resulting spatial distributions of average annual E_a are shown and discussed further in Section 5.1. For comparative average seasonal hydrological calculations (results Section 5.3), seasonal average E_a-values representative for the summer period (June to September) and the winter period (October to May), could not be estimated on the basis of temperatures through Equation (8), because this equation is based on annual mean temperatures. Instead, we assigned seasonal E_a-values corresponding to 57.5% and 42.5%, for the summer and winter period, respectively, of the total annual average E_a-value obtained through method (i). The percentages 57.5% and 42.5% are consistent with the reported evapotranspiration distribution throughout a year for Kalmar, where processed data is available in a study conducted by SMHI, available at web-page *http://www.smhi.se/sgn0102/n0203/manv2003_07.htm*.

4.5 Soil data

Soil input data was derived from the SGU map series "*Jordartsinformation i serie Ae*". Specifically, the SGU classification code "*Klartextbeskrivning J123*" was used, which is a classification based on combined information of the soil surface (<0.5 m; "J1"), the soil upper layer (=0.5 m; "J2") and the deeper soil layer (>0.5 m; "J3"). The soil categories given in "J123" are of mixed type, i.e. some refer to genesis and some refer to texture. However, empirical relations used in the present study (Table 3-1 after /Wendland, 1992/ and Table 3-2 after /Meinardi et al, 1994/), in accordance with the POLFLOW model /De Wit 1999; 2001/ use the soil texture classes "Coarse", "Medium", "Medium fine", "Fine" and "Very fine", and an additional "Water" class. The soil categories of "J123" were therefore translated and reduced to these texture classes (using the PCRaster lookup operator), according to Table 4-1.

We note that /Wendland, 1992/ defined an additional "peat" class, which is lacking in /Meinardi et al, 1994/. For simplicity, we have therefore omitted the peat class in Table 3-1 and use instead the same five classes as in Table 3-2 and /Meinardi et al, 1994/, translating "fen peat" and "bog peat" to the soil texture class "very fine" (Table 4-1; noting also that the coefficients in /Wedland, 1992/ for the "peat" class (not shown in Table 3-1) and the "very fine" soil texture class (shown in Table 3-1) differ by less than 10%).

Table 4-1. Translation of the soil categories in the SGU coding "J123" to the six soil texture classes required by the empirical relations used in this work.

Soil category given in the SGU classification "J123"	Soil texture (translated)
Post-glacial medium sand	coarse
Bedrock	coarse
Post-glacial medium sand with thin surface peat layer	coarse
Coarse silt – Boulder	coarse
Post-glacial gravel	coarse
Post-glacial gravel with thin surface peat layer	coarse
Surge sediment, stone – boulder	coarse
Sandy till	medium
Fillings on unknown subsurface	medium fine
Clayey sandy silty till	fine
Clayey sandy till	fine
Fen peat	very fine
Glacial clay, unspecified with thin surface peat layer	very fine
Glacial clay, unspecified	very fine
Clayey mud – Muddy clay	very fine
Bog peat	very fine
Mud	very fine
Water	water

The distribution of these soil and water classes as derived from the translation (Table 4-1) of the SGU soil type map "*Jordartsinformation i serie Ae*" is shown in Figure 4-4 and influences the following model parameters:

- PS(E_a,P) if E_a is calculated according to method (ii), using Equation (1) and Table 3-1.
- Fraction of deep groundwater recharge (f_{dgw}), according to Table 3-2 and Equation (10); not used for the results presented in this report.

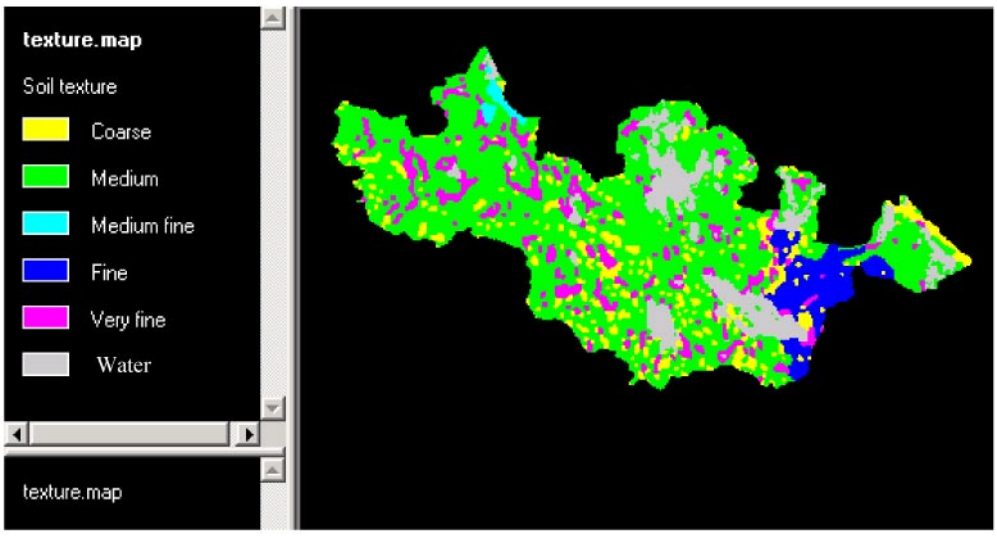

Figure 4-4. *The soil texture map, used as input for the hydrological modelling and derived on basis of the SGU soil type map "Jordartsinformation i serie Ae" translated as in Table 5-1.*

4.6 Land cover (vegetation) data

Groundlayer and vegetation data was provided to us in processed form by SKB as ArcGIS shape files. We combined the information from the original vegetation data map (treelayer_forsmark_025ha.shp), and the original ground layer data map (groundlayer_forsmark_025ha.shp), creating a new land cover data map. Specifically, in the first processing step, the "No_tree" layer was extracted from "treelayer_forsmark_025ha.shp" and added to the layers of "groundlayer_forsmark_025ha.shp" (in cases of conflict overwriting information of the latter map). In the second processing step, the altogether 12 original classes of information were reduced to five new classes following the classification listed in Table 4-2, which was further used as input for the hydrological modelling, determining the coefficients described in Tables 3-1 and 3-2, and Equation (9). The resulting distribution of these five new land cover classes over the Forsmark catchment is shown in Figure 4-5.

Table 4-2. Translation of 12 original vegetation and groundlayer classes to 5 new land cover classes required by the empirical relations used in this work.

Original vegetation and groundlayer class	Land cover class (translated)
Outside mapping area	No Data
Built-up areas, pits etc. (Other)	Built-up
Coastal bare rocks (Other)	Built-up
Arable land (Other)	Open land
No tree area (Added from No_tree-layer)	Open land
Moss type (Forest)	Forest
Peatland – Sphagnum type (Wetland)	Wetland
Peatland – other (Wetland)	Wetland
Not peatland – moss type (Wetland)	Wetland
Not peatland – other (Wetland)	Wetland
Moss type (pastures and meadow) (Other)	Wetland
Water (Other)	Water

The following model parameters are influenced by the land cover:

- $PS(E_a,P)$ if E_a is calculated according to method (ii) below, see Equation (1) and Table 3-1.
- Total fraction of groundwater recharge (f_{gw}), see Equation (9).
- Fraction of deep groundwater recharge (f_{dgw}), see Table 3-2 and Equation (10); not used for the results presented in this report.

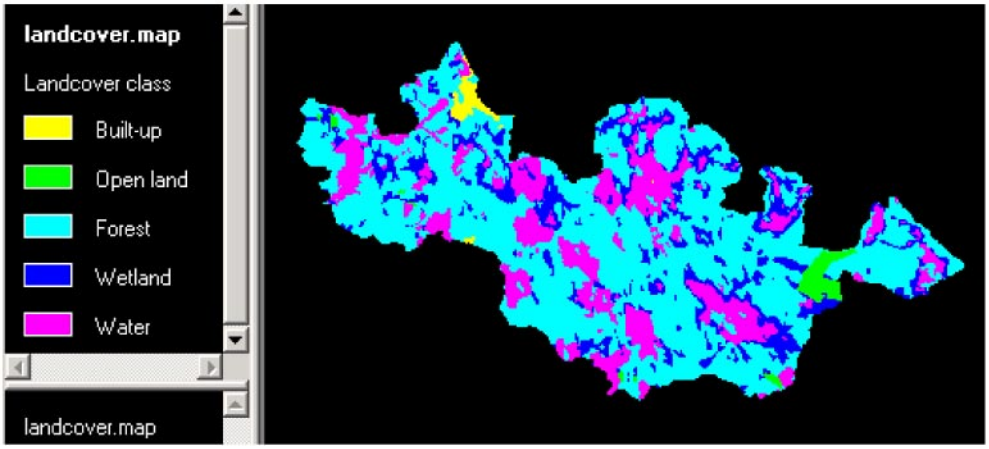

Figure 4-5. *The land cover map, used as input for the hydrological modelling and derived on basis of ground layer and vegetation maps.*

4.7 Aquifer data

The entire model area belongs to the SGU class 1005, Igneous rock, with groundwater flow capacity 600–2,000 (l/h). The aquifer capacity influences:

- Fraction of deep groundwater recharge (f_{dgw}), see Table 3-3 and Equation (10); not used for the results presented in this report.

Furthermore, the aquifer hydraulic conductivity and porosity influence:

- Deep groundwater residence times; not used for the results presented in this report.

5 Application Forsmark: Results

5.1 Precipitation surplus and runoff

In determining the long-term annual average precipitation surplus, we use two independent ways for determining evapotranspiration. In method (i), actual evapotranspiration E_a is estimated using either SMHI's estimates of potential evapotranspiration, E_p, or their measurements of temperature T. In the first case, we used Equation (7), which provides an empirical relation between E_a and E_p. In the second case, we used Equation (8), which quantifies empirically a relation between T and E_p, in combination with Equation (7). The model predictions in both these cases were practically identical. We will therefore for simplicity in the following refer to both these model variations as method (i).

In method (ii), E_a is related empirically to different soil and vegetation conditions, with no explicit account for local temperature variations (see further Section 3.2).

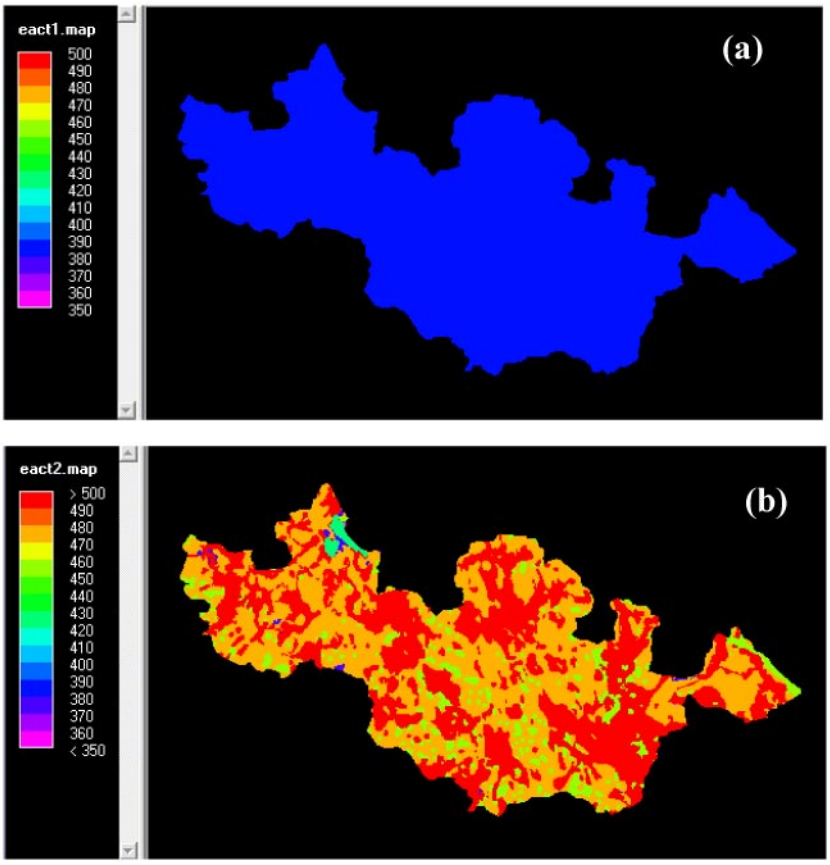

Figure 5-1. *Calculated evapotranspiration (in mm/year) using (a) method (i), and (b) method (ii).*

Figure 5-1a and b show estimates of evapotranspiration E_a using methods (i) and (ii), respectively. Method (ii) (Figure 5-1b) implies a higher degree of local variation, because the underlying local soil and vegetation maps (Figures 4-4–4-5) are much more detailed than the temperature map (Figure 4-3b), which is based on only three measurement stations. There is some degree of local variation also in the Method (i)-prediction (Figure 5-1a), however, because the illustration resolution is, for direct comparison purposes, scaled the same in both Figures 5-1a and b, this smaller variation is not visible in Figure 5-1a. In addition, method (ii) generally predicts higher values of E_a than method (i).

Figures 5-2a and b show the local precipitation surplus (PS), calculated through Equation (1), by use of evapotranspiration methods (i) and (ii), respectively, which also equals total locally created runoff, R, according to Equation (2). Method (ii) generally predicts lower PS and R because its E_a estimates are generally higher (see Figure 5-1).

Furthermore, Figure 5-3 shows the estimated local groundwater recharge index f_{gw}, which is a unique function of the ground surface slope, unless the ground surface is covered with water, or consists of wetlands (Equation (9)). If the land cover is water, f_{gw} is assigned a small value, close to zero, and therefore, lakes appear in pink colour in Figure 5-3.

Finally, Figure 5-4a shows the resulting local groundwater recharge $GW=R_{GW}$ calculated by use of E_a method (i) (PS in Figure 5-2a; f_{gw} in Figure 5-3). In analogy, Figure 5-4b shows the resulting $GW=R_{GW}$ calculated by use of E_a method (ii) (PS-value in Figure 5-2b; f_{gw}-value in Figure 5-3).

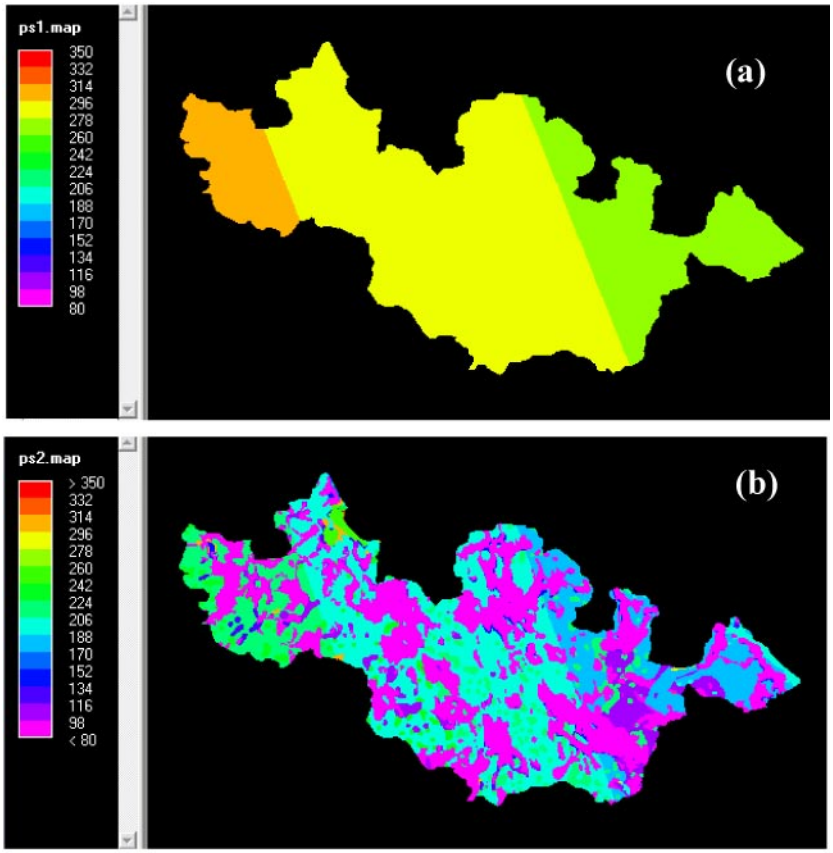

Figure 5-2. *Calculated local precipitation surplus (in mm/year), PS, which also equals total locally created runoff, R (Equation (2)), using (a) evapotranspiration method (i), and (b) evapotranspiration method (ii).*

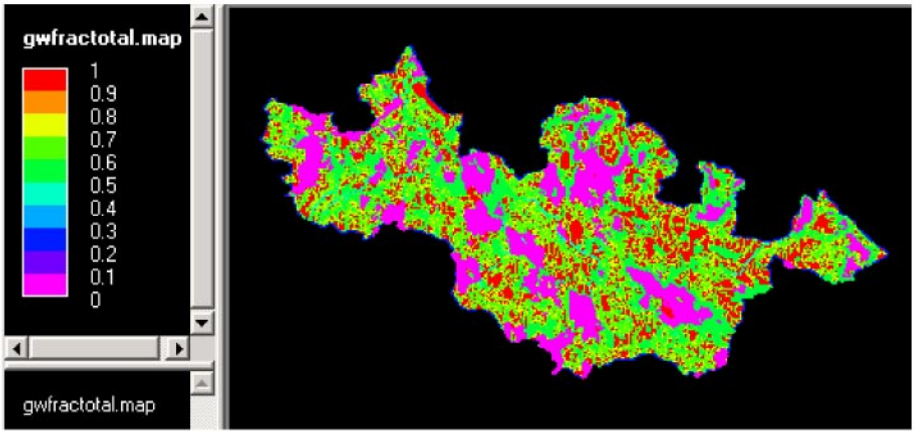

Figure 5-3. *The calculated groundwater recharge index, f_{gw} (dimensionless fraction of precipitation surplus, PS (Figure 5-2); Equation (9)).*

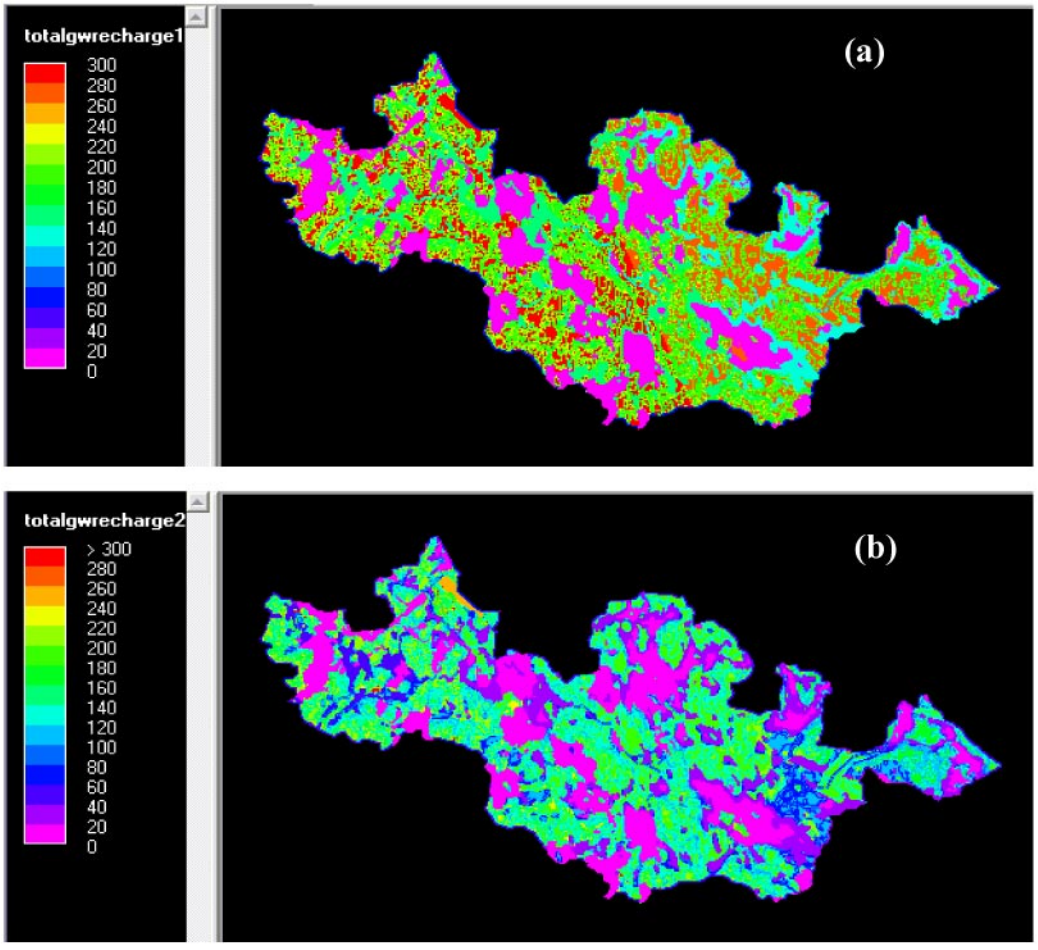

Figure 5-4. *Calculated local groundwater recharge, GW (in mm/year), and corresponding locally created groundwater discharge R_{GW}=GW (Equation (3)), adding to local stream runoff, or flowing as groundwater and adding to stream runoff further downstream (see discussion in Section 3.1), using Equation (3) and (a) E_a-method (i), or (b) E_a-method (ii).*

Averaging the local R values shown in Figure 5-2 over the entire catchment area, we obtain the normalised runoff values presented in Table 5-1. Furthermore, Table 5-2 shows previously reported area-averaged runoff values, for catchments in the vicinity of the modelled Forsmark catchment. The results show that the average reported runoff value of approx. 7.1 l/s/km^2 is well within the herein calculated runoff range given by the E_a-method (i) value (8.8 l/s/km^2) and E_a-method (ii) value (4.6 l/s/km^2).

The average calculated runoff by the two methods of 6.7 l/s/km^2 is also close to the reported 7.1 l/s/km^2-value; this result is consistent with previous experience from the Norrström drainage basin using PCRaster-POLFLOW /Greffe, 2003/, where also totally uncalibrated runoff predictions (as in the present study), using the average E_a value of method (i) and method (ii), were consistent with available observational data of stream flows.

Table 5-1. Modelled area-averaged runoff in the Forsmark catchment using different evapotranspiration estimation methods (i) and (ii).

Runoff per km^2	Prediction method	Main input variable(s)
8.8 l/s/km^2	Method (i)	temperature
4.6 l/s/km^2 l/s/km^2	Method (ii)	soil type and land cover
Average: 6.7 l/s/km^2	–	–

Table 5-2. Measured area-averaged runoff in the Forsmark catchment vicinity.

Runoff per km^2	Location	Reference
6.5 l/s/km^2	Forsmark catchment	P-O Johansson; personal communication
7.7 l/s/km	Gimo station, Östhammar	SKB R-99-70
7.4 l/s/km^2	Fors station, Östhammar	SKB R-99-70
6.6 l/s/km^2	Odenfors station, Tierp	SKB R-99-70
7.6 l/s/km^2	Näs station, Tierp	SKB R-99-70
7.1 l/s/km	Uvlunge station, Tierp	SKB R-99-70
Average: 7.1 l/s/km^2	–	–

5.2 Streamflow distribution among different coastal outlets

Figure 5-5 shows the calculated streamflow, Q (Equation (6), in the 11 coastal stream outlets of the Forsmark catchment (see Figure 4-2) for E_a-method (i) and (ii) along with the total coastal outflow (sum of all outlets). These calculations are based on the local total runoff (equal to local precipitation surplus, Equation (2)) maps shown in Figure 5-2 and Equation (6).

Furthermore, Figure 5-6 shows that E_a-methods (i) and (ii) yield the same relative flows, i.e. the same relative distribution of total flow among the different coastal outlets (and associated sub-catchments) of the total catchment area. Hence, the difference between the methods concerns mainly their mean, or total, outflow estimates, with hardly any difference being exhibited in their resulting spatial distribution of this total/mean outflow.

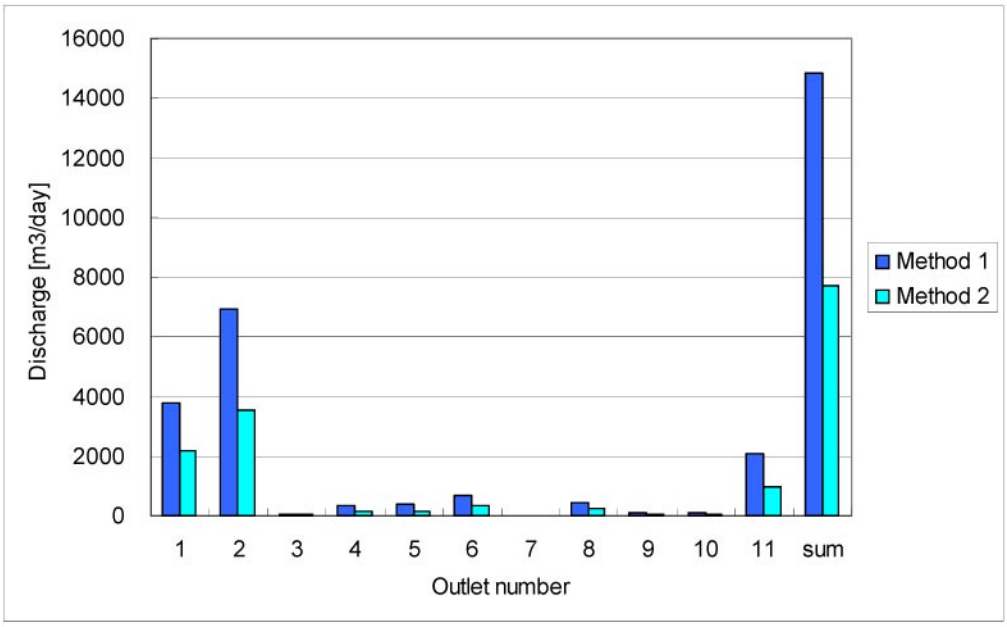

Figure 5-5. *Estimated coastal stream discharge Q (Equation (6)) though the 11 coastal stream outlets within the catchment (see Figure 4-2 for their location), and the total coastal discharge Q_{tot} from the catchment (sum of all 11 outlets), for E_a-method (i) (dark blue bars) and E_a-method (ii) (light blue bars).*

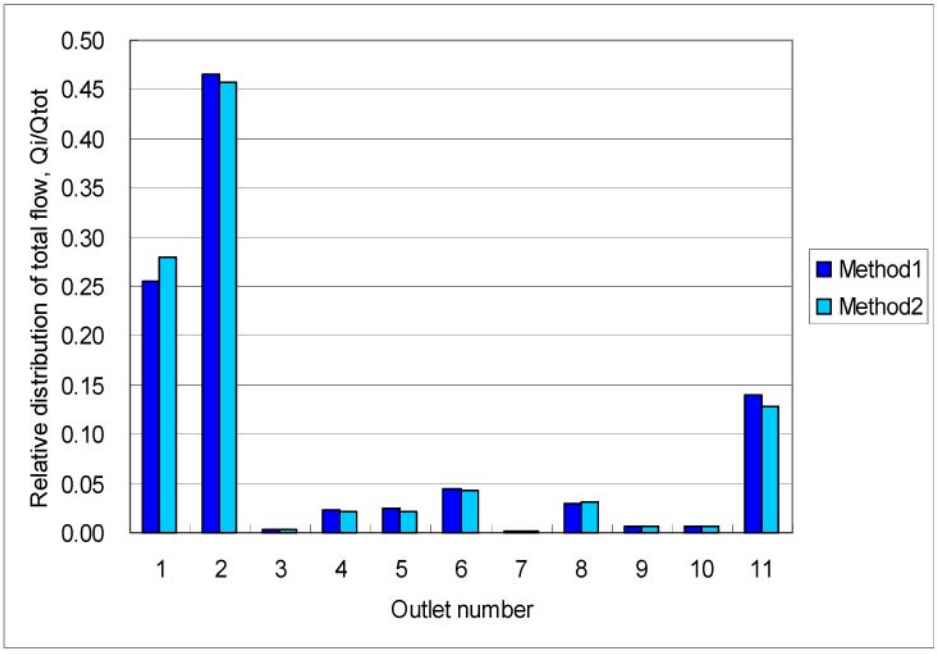

Figure 5-6. *Relative distribution Q_i/Q_{tot} of total flow Q_{tot} (see sum of Figure 4-5) among the different coastal outlets i, for E_a-method (i) (dark blue bars) and E_a-method (ii) (light blue bars).*

5.3 Average seasonal stream flow in coastal outlets

Estimation of average seasonal differences in coastal discharge between summer and winter are shown in Figure 5-7. Since storage through snow accumulation is not included in the model in its present state, we need to define the length of the winter season such that it will fully cover the main snowmelt season and associated average spring flood. Therefore, the considered winter-season is an 8-month period between 1st of October and 31st of May, and the summer season is a 4-month period between 1st of June and 30th of September. Through this definition, the change in snow storage between the beginning and end of each season is expected to be zero on average. Furthermore, we have for simplicity assumed that the total changes in surface water and groundwater storage within each season is small relative to the total precipitation surplus during that season. However, if needed, other assumptions regarding surface water storage is possible within the framework of PCRaster.

Figure 5-7 shows that the calculated average coastal discharge within the summer season (blue bars) is approximately half that of the winter season (grey bars). For direct comparison, the annual average discharge is also shown in Figure 5-7 by the light-yellow bars. The fact that annual average value is closer to the value for the winter season, rather than the summer season, is a consequence of our definition of the winter season as being twice as long as the summer season.

Furthermore, as shown by comparison with available runoff data in the Forsmark catchment vicinity (Tables 5-1 and 5-2), method (i) appears to generally overpredict the average annual precipitation surplus and runoff (with a predicted value of 8.8 l/s/km^2 in comparison with the average measurement value of 7.1 l/s/km^2). It is hence likely that also the uncalibrated estimates of seasonal discharges are biased to a similar extent. However, Figure 5-8 suggests that one single calibration factor would be sufficient to correct for such bias in all 11 coastal outlets. The reason is that the coastal results show the same relative distribution of total flow among the different outlets during both the winter season and the summer season (Figure 5-8). This relative distribution furthermore coincides with the corresponding distribution predicted by the independent E_a-method (ii), as shown in Figure 5-6.

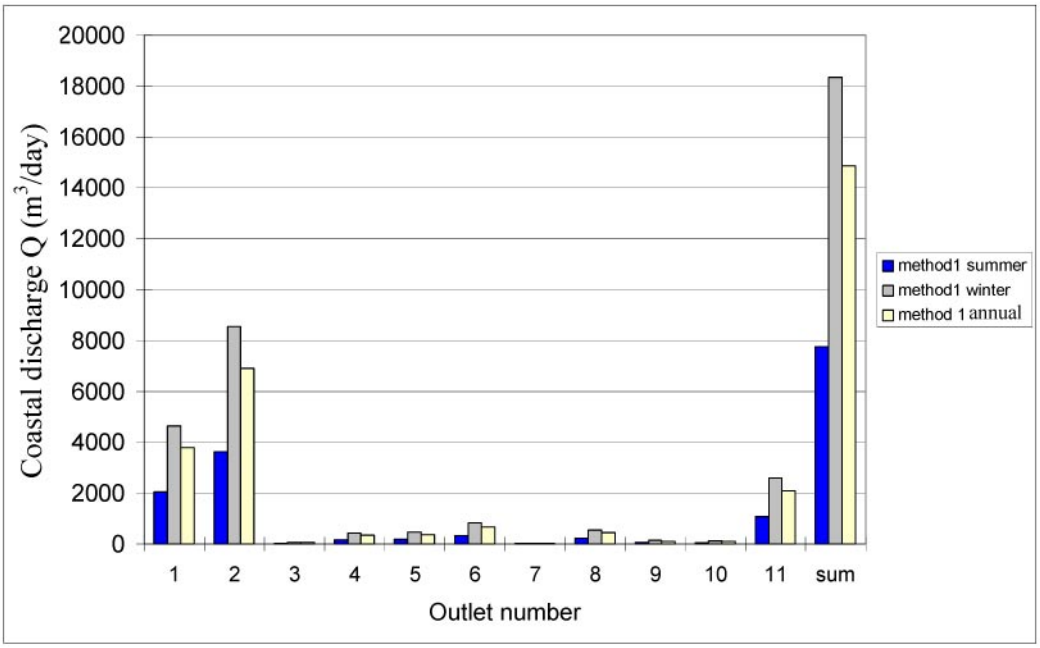

Figure 5-7. *Average, seasonal coastal discharge in summer (blue bars) and winter (grey bars), using method (i). For comparison, the light yellow bars show the annual average discharge values predicted by method (i).*

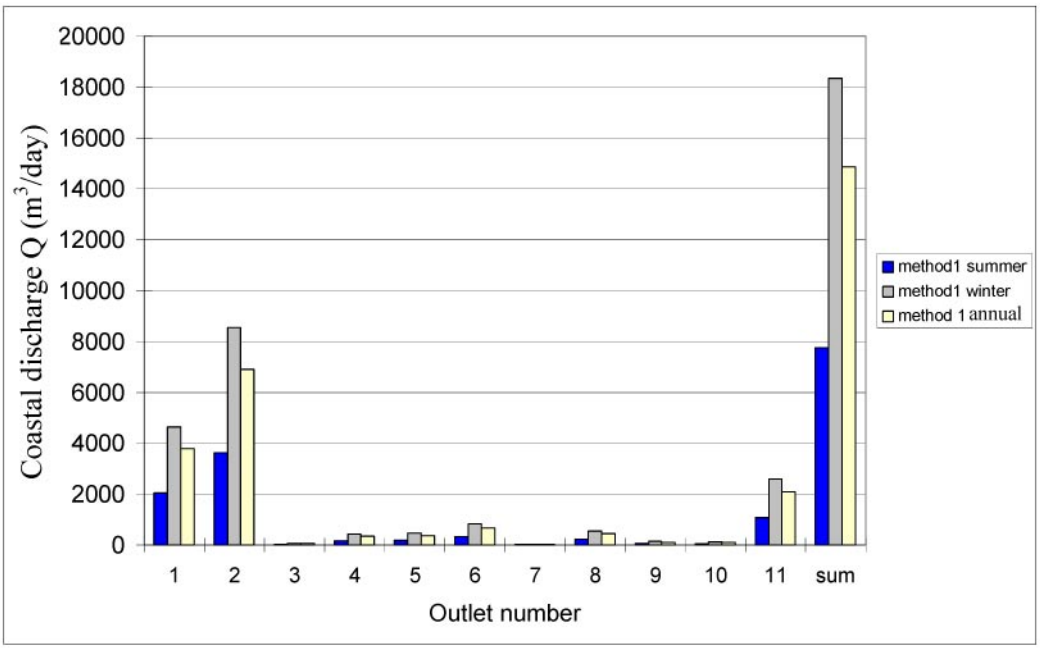

Figure 5-8. *Relative distribution of total average seasonal discharge among the different coastal outlets. The blue bars show results for the summer season (indicated by index s) for each outlet i (Qsi/Qstot, where Qsi is the flow at each coastal outlet and Qstot is the total coastal flow), the grey bars show results for the winter season (indicated by index w; Qwi/Qwtot), and the light yellow bars show results for the average annual discharge (index a; Qai/Qatot).*

5.4 Stream flow in planned measurement stations

The planned location of streamflow measurement stations within the modelled Forsmark catchment is indicated in Figure 4-2. Figure 5-9 shows our expected best estimate of the average annual discharge Q (Equation (6)). This estimate is based on the average value of E_a-estimation method (i) and (ii). Underlying results of estimation methods (i) and (ii) are listed in Table 5-3. As discussed in previous sections and in /Greffe, 2003/, the mean value of (uncalibrated) method (i) and (ii) predictions have been shown to agree well with experimental observations in, e.g. the Norrström catchment, and also appear to reproduce observed, average runoff per km^2 in the Forsmark catchment vicinity.

Regarding the prediction of seasonal, average discharge values, we used the temperature-based method (i) for obtaining results for summer and winter conditions. The results are listed in Table 5-3, and expressed as fractions of the annual, average discharge. The value of about 53% for the summer season hence implies that the streamflow during an average summer day (between June and September) is expected to be 53% of the annual, average streamflow. In analogy, the value of about 123% for the winter season implies that the streamflow during an average winter day (between October and May) is expected to be 123% of the annual, average streamflow. As shown in Table 5-3, the seasonal variation is expected to be similar at all measurement points.

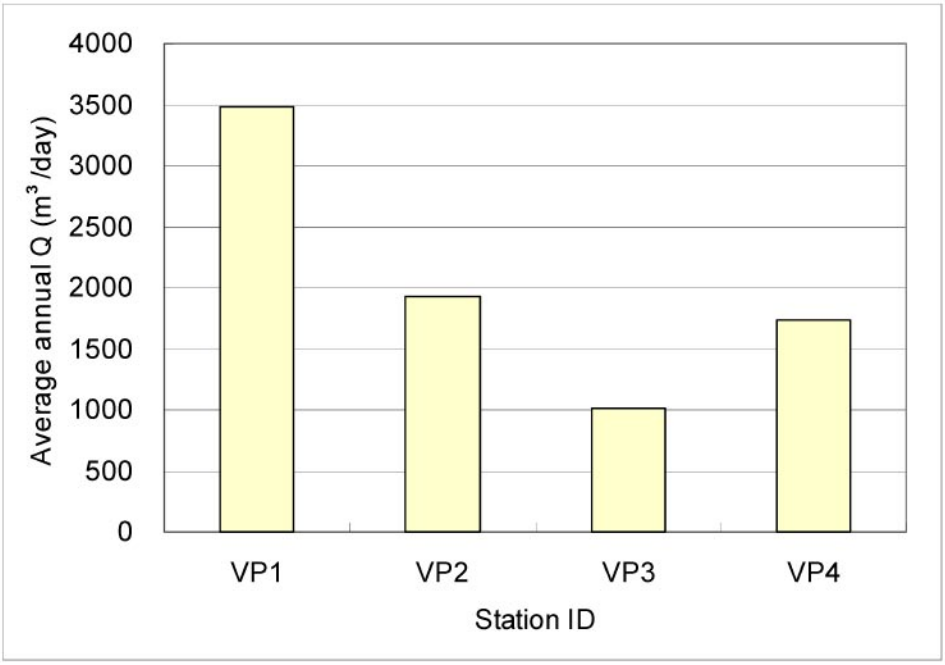

Figure 5-9. *Predicted average annual discharge Q at planned measurement stations VP1–VP4 (expected best estimate; average of E_a-methods (i) and (ii)).*

Table 5-3. Expected best estimate of average annual discharge Q (also shown in Figure 5-9), compared to average annual discharge for E_a-method (i), average annual discharge for E_a-method (ii), and average seasonal relative to average annual discharge during summer and winter seasons.

		Measurement station (Figure 4-2)			
	Unit	**VP1**	**VP2**	**VP3**	**VP4**
Annual, average discharge (average value of method (i) and (ii), shown in **Figure 5-9**)	(m^3/day)	**3480**	**1930**	**1010**	**1730**
Annual, average discharge, *method (i)*	(m^3/day)	4570	2560	1340	2220
Annual, average discherge, *method (ii)*	(m^3/day)	2390	1300	690	1230
Average seasonal relative to average annual discharge during **summer** season (June to September)	(–)	**0.53**	**0.53**	**0.53**	**0.54**
Average seasonal relative to average annual discharge during **winter** season (October to May)	(–)	**1.23**	**1.23**	**1.23**	**1.22**

6 Discussion

6.1 General

In general, we have used the modelling approach without consideration of transient effects, which would for instance require handling of water storage changes. For calculations of average seasonal conditions (summer and winter), we defined the seasons such that snow melt and spring flood on the average should occur completely within the an eight-month long winter season, thus avoiding the problem of snow storage in between seasons. If finer temporal resolution is required, the model needs to be extended such that it accounts for storage effects. We expect that this can be accomplished through relatively minor changes of the present modelling scheme.

Overall, the application of the PCRaster-POLFLOW modelling approach to the Forsmark area showed results that were in good agreement with available average runoff values. The runoff prediction may be considered to constitute the core of the current PCRaster-POLFLOW model, however, the present modelling exercise also provided insights into possible ways of extending and improving the model. In particular, possible couplings to groundwater and solute transport modelling are discussed in Section 6.2 and the possible reduction of uncertainties related to estimation of actual evapotranspiration is discussed in Section 6.3.

6.2 Groundwater – surface water interactions and solute transport

The present modelling is based on the determination of spatially distributed precipitation surplus (PS), derived from the difference between precipitation and actual evapotranspiration in each grid cell (Equation (1)). In a subsequent modelling step, the fraction of this PS that recharges groundwater is calculated through the groundwater recharge index f_{gw} (Equation (9)). Under zero-storage (steady-state) conditions, this groundwater recharge must lead to an equal amount of groundwater discharge, either into local (within cell) streams, or as groundwater flow in downstream cells and their streams, as discussed in more detail in Section 3.1. A possible means of handling the groundwater storage problem under non-steady conditions is to simulate more detailed groundwater flow separately and off-line, adopting an iterative procedure.

Furthermore, the present PCRaster-POLFLOW modelling procedure assumes that the mean groundwater flow direction is determined from the topographic ground surface slope. Significant differences between local groundwater and surface water flow directions, however, may arise, for instance, if the terrain is flat, the recharge is relatively large (such that it influences hydraulic gradients and hence the location of the groundwater divide), or the groundwater is relatively deep. Such differences may significantly affect the distribution of water between different sub-catchments and streams, and can also be considered through a separate, more detailed and iterative handling of groundwater flow conditions.

For making such an iterative coupling of PCRaster-POLFLOW and a groundwater modelling tool practically feasible, the groundwater module should be able to use PCRaster-POLFLOW output as well as GIS information, be relatively quick in obtaining a numerical solution, and provide results in a format that readily can be handled by PCRaster-POLFLOW and GIS interfaces. We believe that a suitable model and interface having these abilities are the Analytic Element Method /AEM; Strack, 1999; 2003/ in combination with its user-friendly pre- and post processor ArcFlow, developed by the groundwater research group at the University at Buffalo, New York.

A preliminary test of the AEM-ArcFlow capabilities was conducted at Stockholm University in collaboration with K. Bandilla, visiting Ph.D. student from the University at Buffalo. The AEM-ArcFlow model was then given the same basic input data for the Forsmark catchment as used in this study. Results showed that AEM-ArcFlow could readily provide solutions for groundwater flow, flow paths and advective travel times using this input (and providing output in a PCRaster-POLFLOW compatible format) through, for instance, generating relevant hydraulic head boundaries based on available stream network and elevation data.

If solute transport modelling is of main interest, such as that of radionuclides entering the coupled shallow groundwater – surface water hydrological system from possible deep repository leakage, the recent semi-analytical approach of /Lindgren et al, 2004/ to modelling solute transport through the integrated groundwater – stream system of a catchment may, for instance, be a fruitful tool to use in combination with the PCRaster-POLFLOW surface-hydrological approach. This combination can be made in terms of solute travel time distributions, which can be obtained from the PCRaster-POLFLOW model for the surface – hydrological system and coupled to relevant groundwater travel time distributions for different possible groundwater source scenarios by use of the methods outlined by /Lindgren et al, 2004/.

The latter coupling methods have already been shown to be useful for reactive solute transport, subject to irreversible degradation or decay /Lindgren and Destouni, 2004/. In parallel, /Darracq and Destouni, 2004/ have also demonstrated the PCRaster-POLFLOW model's capability of addressing the same reactive transport problem by explicit calculations of solute travel times in combination with irreversible degradation / decay rates in the surface – hydrological system. We believe that a combination and further development of these two modelling approaches may be very relevant and useful for developing necessary site-specific models of coupled groundwater-surface water hydrology and reactive solute transport.

With regard to reactive transport, /Malmström et al, 2004/ have also very recently demonstrated the possibility to couple complex multi-component reaction systems, modelled by the widely used geochemical model PHREEQC /Parkhurst and Appelo, 1999/, with solute travel time distributions, derived for instance by the PCRaster-POLFLOW model and the model of /Lindgren et al, 2004/ for different hydrological sub-systems of a catchment.

6.3 Evapotranspiration modelling

6.3.1 Land cover related models

With land cover-related models, we mean models that quantify evapotranspiration E_a based on information on properties of the ground system itself and its vegetation. For instance, the coupled heat and mass transfer model for soil-plant-atmosphere systems /the Coup model; Jansson and Karlberg, 2001/ addresses the physics of heat and evaporative flows, considering a depth-profile of the soil-plant system, which may contain isolated as well as competing plant communities. However, it requires local information on soil layer properties (e.g. the water retention curves and heat capacities), plant properties (e.g. vertical root distributions, and resistance for water flow between plant and atmosphere), and time-series of meteorological variables (e.g. precipitation, air temperature, air humidity, wind speed and cloudiness). This limits its practical use at catchment/regional scales, unless the region is characterized in appropriate spatial and temporal detail, which would be both observationally and computationally very resource demanding.

For quantifications at the catchment-regional scales, numerous empirical models have been developed, which account for various ambient and boundary conditions without attempting to reproduce in detail the underlying physical processes. The HBV hydrological model developed by SMHI, for instance, uses long-term mean potential evapotranspiration based on the Penman formula /Penman, 1948; see also Lindström et al, 1997/.

In the present study, we used two alternative formulations for the actual evapotranspiration, E_a. The first method (method (i); /Langbein, 1949; Turc, 1954; Meinardi, 1994/) accounts explicitly for the effect of annual mean temperature on E_a, whereas the effects of soil and vegetation are accounted for only implicitly, assuming that these effects are similar in different applications. By contrast, in the second method (method (ii); /Wendland, 1992/), E_a is related empirically to different soil and vegetation conditions, whereas there is no explicit account for temperature effects, which are assumed to be similar in different applications. A plausible explanation for the deviations in the present results between methods (i) and (ii), is that (at least one of) these assumptions are relatively inaccurate. For instance, method (ii) was developed for temperature-ranges characteristic of Germany, and it is likely that included empirical coefficients must be modified before application in other areas.

However, we also show in the result sections that the two considered evaporation models yield the same results in terms of the relative distribution of coastal flows from the catchment. This implies that the model can readily be calibrated by use of one single calibration factor for adjustment of E_a on the basis of one streamflow observation in any of the different catchment outlets. Moreover, empirical evidence from other applications in Sweden of models (i) and (ii) shows the average value of their predictions to be consistent with measurements /Greffe, 2003; Darracq, 2003/. It is based on that experience that we also made predictions for planned measurement stations in Forsmark (Section 5.4), without using one single catchment-specific model calibration factor.

Since land-cover related E_a-models for application on the catchment scale generally depend on classification of, and calibration to, local characteristics (regarding, e.g. the evaporative properties of the soil and the surface), we do not believe that any empirically-based model can provide more predictive strength, without considerable site-specific adaptations, than that demonstrated here, for the PCRaster-POLFLOW model, regarding average seasonal, or annual, values of E_a. However, if greater spatial or temporal detail is needed, we suggest the use of remote sensing models for E_a-estimation (discussed in the following), because they involve measurement of parameters that directly govern heat and evaporative flows, decreasing for instance the uncertainties related to vegetation, soil and surface properties classifications.

6.3.2 Remote sensing models

In remote sensing hydrological models, spatially distributed E_a-values are determined from spectral satellite data using an energy balance approach. The Surface Energy Balance for Land model /SEBAL; Bastiaansen et al, 1998a; 1998b/ has been applied and validated on scales ranging from less than one square kilometre (for a single site; /Hemakumara et al, 2003/), to about one thousand square kilometres (for a whole catchment or region; e.g. /Ayenew, 2003; Chemin et al, 2004/). It has further been applied to crops, pastures, forests, natural vegetation, mixed vegetation, bare soil, desert and open water bodies /Bastiaansen, 2000; Hemakumara et al, 2003/.

For the estimation of E_a, the SEBAL model calculates surface temperature, vegetation index (e.g. the so-called normalized difference vegetation index; NDVI), emissivity and albedo, on the basis of different spectral bands of satellite data. It furthermore relies on some complementary ground data, such as the incoming short-wave and long-wave radiation (which, in absence of radiation measurements, can be estimated from the hours of sunshine in combination with air temperature and air humidity) and wind speed. The resolution of satellite images that have been used in SEBAL applications ranges from about 30m×30m with Landsat 7ETM+ and Landsat 5TM images to 1.1 km×1.1 km with NOAA AVHRR images that are freely available on the internet (see summary of /Chemin et al, 2004/).

The main limitations of the SEBAL E_a model are that the influence of surface roughness is poorly described and that it is mainly suitable for relatively flat terrain /Bastiaanssen et al, 1998a/. Furthermore, cloud-free conditions are required. Its main advantages are that it is based on physical concepts, and therefore applicable for various climates, that it does not rely on land use classification, and that it can be applied at different spatial and temporal resolutions /Bastiaanssen et al, 1998a/. For instance, one satellite image can yield a daily, average E_a-value, whereas seasonal E_a-values can be obtained by adding satellite images together following a weight ratio based on the length of the time period separating two consecutive images /Chemin et al, 2004/.

A comparison between SEBAL estimates of E_a and ground-based large aperture scintillometer (LAS) estimates of E_a for a mixed vegetation test site in Sri Lanka showed that whereas the estimations between the two methods differed by 17% considering a 10-day period, this difference decreased to 1% when monthly estimates where considered /Hemakumara et al, 2003/. Regarding the time required for processing of raw satellite data, /Bastianssen, 2000/ reports that a professional analyst needs one day for each Landsat image.

7 Conclusion summary

The PCRaster-POLFLOW modelling approach has previously been applied at relatively large river basins and catchments, such as Rhine, Elbe, and Norrström /De Wit 1999; 2001; Greffe, 2003; Darracq 2003/. In this study, we apply the modelling approach using a relatively fine spatial resolution to the smaller catchment of Forsmark. The main conclusions are:

- On the basis of totally uncalibrated site-specific model input parameters for the Forsmark catchment, the GIS-based surface hydrologic PCRaster-POLFLOW model yielded area-averaged runoff results values that agree well with available, independent hydrologic runoff data.
- Predicted average annual stream flow values have been delivered for four planned hydrological stations within the Forsmark catchment, thus allowing for future direct comparisons with streamflow monitoring.
- We showed that, and how, the PCRaster-POLFLOW model even in its present state can be used for predicting average seasonal streamflow. Results for summer and winter seasons showed that, whereas there are differences in the absolute streamflow values between the seasons, the relative distributions of flow between different coastal stream outlets are the same for average seasonal and annual conditions.
- On the basis of the present analysis we have identified possible fruitful ways of model development with respect to the critical evapotranspiration modelling.
- On the basis of the present analysis in combination with other related and very recent results on the modelling of solute transport in the integrated groundwater-stream system of a catchment, we have also identified possible fruitful ways forward for realistic coupled modelling of groundwater-surface water interactions and reactive solute transport in catchments.

8 References

Ayenew T, 2003. Evapotranspiration estimation using thematic mapper spectral satellite data in the Ethiopian rift and adjacent highlands. *Journal of Hydrology*, 279, 83–93.

Bastiaanssen W G M, 2000. SEBAL-based sensible and latent heat fluxes in the irrigated Gediz Basin, Turkey. *Journal of Hydrology*, 229, 87–100.

Bastiaanssen W G M, Menenti M, Feddes R A, Holtslag A A M, 1998a. A remote sensing surface energy balance algorithm for land (SEBAL). 1. Formulation. *Journal of Hydrology*, 212–213, 198–212.

Bastiaanssen W G M, Pegrum H, Wang J, Ma Y, Moreno J F, Roerink G J, van der Wal T, 1998b. A remote sensing surface energy balance algorithm for land (SEBAL). 2. Validation. *Journal of Hydrology*, 212–213, 213–229.

Chemin Y, Platonov A, Ul-Hassan M, Abdullaev I, 2004. Using remote sensing data for water depletion assessment at administrative and irrigation-system levels: case study of the Ferghana Province of Uzbekistan, *Agricultural Water Management*, 64, 183–196.

Darracq A, Greffe F, Hannerz F, Destouni G, Cvetkovic V, 2003. Nutrient transport scenarios in a changing Stockholm and Mälaren valley region. *Proceedings 7th International Specialised Conference on Diffuse Pollution and Basin Management*, Dublin, 17th–22nd August 2003.

Darracq A, 2003. *Dynamic characterization of nutrient transport in the Norrström drainage basin.* TRITA-LWR Master Thesis, Dept of Land and Water Resources Engineering, KTH, Stockholm.

Darracq A, Destouni G, 2004. In-stream nitrogen attenuation: model artifacts and management implications for coastal nitrogen impacts. *Environmental Science and Technology* (in review).

De Wit M, Meinardi C, Wendland F, Kunkel R, 2000. Modelling water fluxes for the analysis of diffuse pollution at the river basin scale. *Hydrological Processes*, 14, 1707–1723.

De Wit M J M, 1999. *Nutrient fluxes in the Rhine and Elbe basins*. Ph.D. Thesis, Utrecht University, *NGS Publication* 259, 163 pp.

De Wit M J M, 2001. Nutrient fluxes at the river basin scale. I: the PolFlow model. *Hydrological Processes*, 15, 743–759.

Greffe F, 2003. *Material transport in the Norrström drainage basin: Integrating GIS and hydrological process modeling.* TRITA-LWR Master Thesis, Dept. of Land and Water Resources Engineering, KTH, Stockholm.

Hemakumara H M, Chandrapala L, Moene A F, 2003. Evapotranspiration fluxes over mixed vegetation areas measured from large aperture scintillometer. *Agricultural Water Management*, 58, 109–122.

Jansson P-E, Karlberg L, 2001. *Coupled heat and mass transfer model for soil-plant-atmosphere systems*. Royal Institute of Technology, Dept of Civil and Environmental Engineering, Stockholm 325 pp. (internet-page ftp://www.lwr.kth.se/CoupModel/CoupModel.pdf).

Langbein W B, 1949. *Annual runoff in the United States.* U.S. Geological Survey Circular 52, U.S. Dept. of the Interior: Washington D.C.

Lindgren G A, Destouni G, 2004. Nitrogen Loss Rates in Streams: Scale-Dependence and Up-Scaling Methodology. *Geophysical Research Letters* (in press).

Lindgren G A, Destouni G, Miller A V, 2004. Solute transport through the integrated groundwater-stream system of a catchment, *Water Resources Research*, 40, doi:10.1029/2003WR002765.

Lindström G, Johansson B, Persson M, Gradelin M, Bergström S, 1997. Development and test of the distributed HBV-96 hydrological model. *Journal of Hydrology*, 201, 272–288.

Malmström M E, Destouni G, Martinet P, 2004. Modeling expected solute concentration in randomly heterogeneous flow systems with multicomponent reactions. *Environmental Science and Technology*, 38, 2673–2679.

Meinardi C, Beusen A, Bollen M, Klepper O, 1994. Vulnerability to diffuse pollution of European soils and groundwater. *National Institute of Public Health and Environmental Protection (RIVM) Report 4615001002*, Bilthoven, The Netherlands.

Parkhurst D L, Appelo C A J, 1999. User's guide to PHREEQC (version 2). *USGS Water-Resources investigations report* 99-4259, USGS, Denver, Colorado, USA.

Penman H L, 1948. Natural evapotranspiration from open water, bare soil and grass. *Proc. R. Soc. London Ser. A.* 193, 120–145.

Rhén I, Follin S, Hermanson J, 2003. Hydrogeological Site Descriptive Model – a strategy for its development during Site Investigations, *SKB R-03-08*, Svensk Kärnbränslehantering AB.

Strack O D L, 1999. Principles of the analytic element method. *Journal of Hydrology* 226, 128–138.

Strack O D L, 2003. Theory and applications of the analytic element method. *Reviews of Geophysics, 41*, doi:10.1029/2002RG000111.

Turc L, 1954. The water balance of soils. Relation between precipitation, evaporation and flow. *Annales Agronomiques* 5: 491–569.

Van Deursen W P A, 1995. Geographical information systems and dynamic models; development and application of a prototype spatial modelling language. Ph.D. Thesis, Utrecht University, *NGS Publication* 190, 206 pp (Electronically available through www.carthago.nl).

Wendland F, 1992. *Die Nitratbelastung in den Grundwasserlandschaften der "alten" Bundesländer (BRD). Berichte aus der Okologischen Forschung*, Band 8, Forschungszentrum Jülich: Jülich; 150 pp.